Plasma Assisted Supersonic Jet Deposition for thin film growth

R. Barni[1], H. Zaka[1,2], I. Amjad[1], C. Riccardi[1]

[1]*Dipartimento di Fisica G. Occhialini, Università degli Studi di Milano-Bicocca, I-20126 Milano, Italy*

[2]*Department of Physics, Faculty of Education, Ain Shams University, Cairo 11566, Egypt*

Thin films, ranging from atomic layers up to micrometers thick, are crucial in high-tech industries, especially when built from particles smaller than 100 nm, giving rise to nanostructured films with new properties respect to bulk materials [1]. Controlled material synthesis achieved via Chemical Vapor Deposition (CVD) or Physical Vapor Deposition (PVD) techniques is very important, to design film properties suitable for diverse applications. Plasma enhanced PE-CVD is a version of such techniques involving plasma technologies.

We proposed a modified method for thin film growth, Plasma Assisted Supersonic Jet Deposition (PA-SJD) [2], whose main improvement consists in the separation of the gas precursor material synthesis phase from the transport to the substrate and to the growing film environment. Using a supersonic jet allows also a better kinetic energy and cluster arrangement control of the flow on the substrate respect to conventional CVD/PVD methods. It offers chemistry control in a reactive cold plasma environment and assembly control with a supersonic inseminated jet over a substrate. The reactor uses a vacuum system with separate plasma and deposition chambers connected by a circular nozzle. A pressure gradient forms between the chambers to induce supersonic jet formation. Plasma generation in the first chamber allows to produce constituents for the thin film growth by dissociating a gaseous precursor injected in the gas-phase of an inductively coupled RF discharge. Dissociated seeds move within the expanding supersonic jet to the deposition chamber, hitting the substrate. Within the supersonic jet, as particles accelerate, pressure and density drop, resulting in a low-collisional, energetic and directional flow.

Thanks to PA-SJD technique we can employ dense plasma for fast deposition which is hardly possible yet with traditional PE-CVD techniques. Here we present some results that were obtained using plasma diagnostics, using mass as well as optical emission spectroscopic (MS/OES) techniques, in order to characterize the plasma state and the supersonic jet, together with its interaction with the substrate. Silica-like thin films were deposited on PET sheets using oxygen and HMDSO. The sheets were positioned at different distances from the nozzle orifice (10 or 15 mm). In Figure 1 a sketch of the supersonic jet development is presented. Empirical

equations determine Mach disk position Z(M) and diameter D(M) based on orifice diameter d_n and pressure ratio between the vacuum chambers up- and down-stream R [2]:

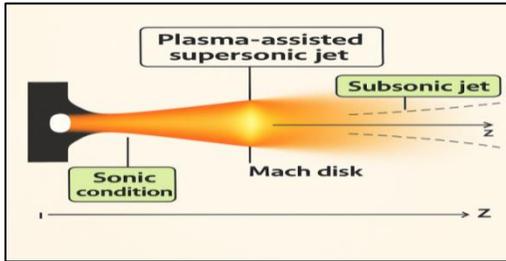$$Z(M) = 0.67 * d_n * \sqrt{R}, \quad D(M) = d_n * (0.36 * R^{0.6} - 0.59)$$

Figure 1: Schematic diagram displays jet expansion in the supersonic nozzle with Mach number variations, Mach disk location, and nozzle diameter.

OES was used during the plasma treatment of PET by pure O2. Spectra of the oxygen plasma are dominated by the emission lines of atomic oxygen and molecular ions O_2^+ [3,4]. Some properties of the supersonic jet could be inferred by measuring the ratio between two different emission lines. In Figure 2, the ratio between the atomic oxygen line at 777 nm emission intensity and five of the molecular ions lines is plotted as a function of the axial distance from the orifice in the plasma jet (Fig.2a) and of the radial distance perpendicular to the jet axis (Fig.2b). Since the lifetimes of all those excited states is very short, the ratios reflect local changes in the plasma properties that modify their population and possibly the concentration of different neutral or charged species. Axial profiles show a decrease from the orifice exit with at least two steps in the plasma conditions approaching the substrate. Radial profiles reveal that plasma conditions are different in the central region of the jet, corresponding to roughly the orifice diameter, respect to the outer ring. A detailed radiative model is needed to extract the characteristics of the plasma state, namely the electron temperature and density. In Figure 3, some results are presented from OES in an experiment with a mixture of O_2 and HMDSO. The emission spectra show again the lines from excited atomic oxygen, but also several new features states indicating the monomer dissociation.
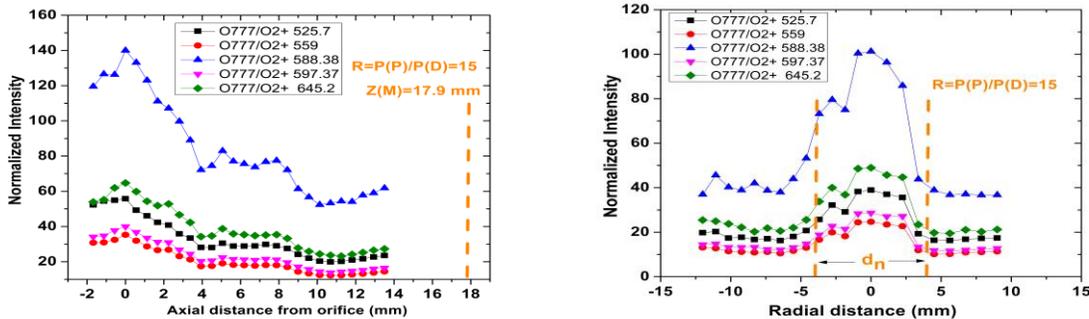

Figure 2: Normalized intensity of O-777 nm line to various ionic oxygen lines shown against plume axial (a) and radial (b) coordinates (Q = 50 sccm, P = 100 W, R = 15, P(D) = 7.4 × 10⁻³ mbar).
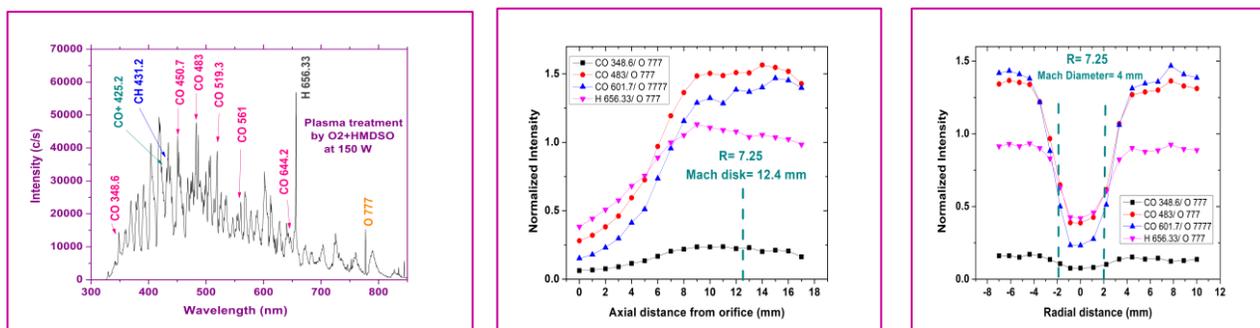
Figure 3: (a) OES analyzed discharge spectrum in a 150 W plasma in oxygen $(P(D) = 6.07 \times 10^{-3}$ mbar, $Q = 40$ sccm) and HDMSO $(P(D) = 6.71 \times 10^{-3}$ mbar). Axial (b) and radial (c) jet profiles of the intensity ratios.

Atomic hydrogen Balmer H_α line (656.3 nm) testifies methyl group hydrogen abstraction. More complete HMDSO dissociation is attested by the emission from CO (450–600 nm) and CH (431 nm) states. The former points also to the oxidation of organic groups, which is relevant to identify conditions leading to pure silica film deposition [3-4]. Figure 3b and 3c show the axial and radial profiles of the jet during a treatment of PET sheets with O_2/HMDSO plasma. Again emission lines intensity ratios are sensitive to the local changes in the plasma underlining properties. Oxidation and dissociation increase, reaching a plateau after a distance roughly corresponding to the nozzle diameter, but have no discontinuities before and after the Mach disk position (here at 12.4 mm), indicating a smooth gas flow transition. There is also some hint that the OES pattern from the region of the film growth, just above the PET surface is slightly different. This arises from the interplay between the diffusion process of components from the plasma jet and the formation mechanism of the film, which could lead to some back-diffusion into the plasma gas-phase. The radial profile pattern correlates well with the expected Mach disk diameter, separating the jet from the surrounding gas-phase, which hosts a diffuse plasma too.
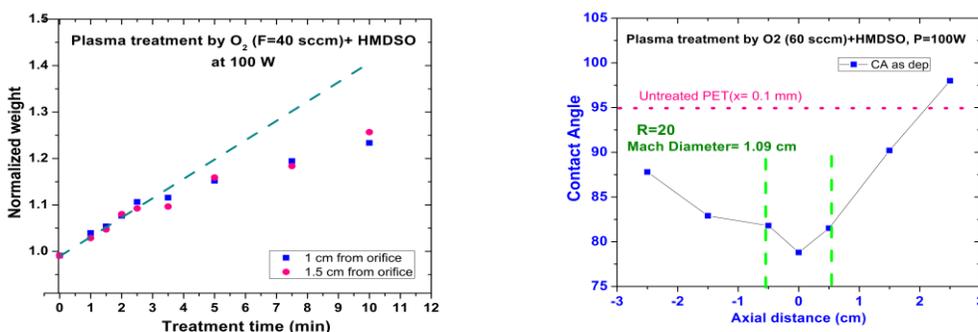

Figure 4: (a) Normalized weight changes as a function of the exposure time to a 100 W plasma jet. Treated PET water contact angle measurements as a function of the distance from the jet axis impact point.

Finally we discuss some properties of the thin film deposited on the PET substrates. Figure 4a shows the sample weight after different exposure times in front of the supersonic jet, for a 100 W discharge. From it, one should infer that the deposition rate is constant, up to uptake quite significant and declines only for longer exposure times, reflecting a change in the growth process, possibly due to the sheer film thickness and/or heating of the substrate region, under the load of the jet flow. As to have a comparison the treated sample was a PET sheet 40x20 mm with a 0.05 mm thickness and 1.35 g/cm^3 density. Figure 4b displays the water contact angle measured on the plasma-treated PET surface, using 3 µL water droplets, with varying distances from the center of the plasma jet, thus mapping the film properties. The untreated PET has a contact angle of 95°. Inside of the Mach disk diameter, where the jet directly impact the PET surface, the contact angle was slightly but significantly decreased, maximally near the jet axis intersection point. The reported increased hydrophilicity is consistent with a silica-like composition of the film, with little retention of organic groups [5]. It is clear that the effect of the plasma exposure extends also outside the Mach disk, where however the modification is not uniform.

Acknowledgements

References

[1] H. Biederman, Plasma Polymer Films, World Scientific (2004).

[2] I. Biganzoli, et al., Journal of Modern Physics 3, 1626-38 (2012).

[3] R. Pearse, A. Gaydon, The Identification of Molecular Spectra, Wiley (1976).

[4] R. Barni, H. Zaka, D. Pal, I. Amjad, C. Riccardi, Photonics 12, 595.1-18 (2025).

[5] E. Blanchard, et al., Langmuir 31, 12944-12953 (2015).